Research Square

Preprints are preliminary reports that have not undergone peer review.
They should not be considered conclusive, used to inform clinical practice,
or referenced by the media as validated information.

Scalable Room-Temperature Synthesis of Glass-like MOF Thin Films on Arbitrary Substrates with Versatile Functionality

Yan Lu

yan.lu@helmholtz-berlin.de

Helmholtz-Zentrum Berlin f&#x00FC https://orcid.org/0000-0003-3055-0073

Wei Zhang

Shanghai University https://orcid.org/0000-0002-4840-8174

Sijia Cao

Helmholtz-Zentrum Berlin fü

Yanchen Liu

Humboldt-Universität zu Berlin

Qingping Wu

Helmholtz-Zentrum Berlin fü

Zibo Zhang

University of Science and Technology Liaoning

Martin A. Karlsen

Deutsches Elektronen-Synchrotron DESY

Liqiang Lu

Helmholtz-Zentrum Berlin fü

Pinna Nicola

Humboldt-Universität zu Berlin: Humboldt-Universitat zu Berlin https://orcid.org/0000-0003-1273-803X

Article

Keywords:

Posted Date: November 16th, 2026

DOI: https://doi.org/10.21203/rs.3.rs-11682154/v1

License: This work is licensed under a Creative Commons Attribution 4.0 International License.
Read Full License

Additional Declarations: There is **NO** Competing Interest.

Scalable Room-Temperature Synthesis of Glass-like MOF Thin Films on Arbitrary Substrates with Versatile Functionality

Wei Zhang [a,b,e]*, Sijia Cao,[b] Yanchen Liu,[e] Qingping Wu,[b] Zibo Zhang,[b,g] Martin A. Karlsen[f], Liqiang Lu[b], Nicola Pinna[e] and Yan Lu [b,c,d]*

a. Key Laboratory of Organic Compound Pollution Control Engineering (MOE), School of Environmental and Chemical Engineering, Shanghai University, Shanghai 200444, China.
b. Institute of Electrochemical Energy Storage, Helmholtz-Zentrum Berlin für Materialien und Energie, Berlin 14109, Germany.
c. Institute for Technical and Environmental Chemistry, Friedrich-Schiller-Universität Jena, Jena 07743, Germany.
d. Helmholtz Institute for Polymers in Energy Applications Jena (HIPOLE Jena), 07743 Jena, Germany.
e. Department of Chemistry and The Center for the Science of Materials Berlin, Humboldt-Universität zu Berlin, Berlin 12489, Germany.
f. Deutsches Elektronen-Synchrotron DESY, Notkestr. 85, 22607 Hamburg, Germany
g. School of Chemical Engineering, University of Science and Technology Liaoning, Anshan 114051, China

Email: weizhang88@shu.edu.cn; yan.lu@helmholtz-berlin.de

Abstract

Metal-organic framework (MOF) glasses and glass-like materials offer unique advantages including improved flexibility, processability and mechanical stability, yet the rational, mild and scalable synthesis of uniform, large-area glassy MOF thin films remains largely unexplored and highly challenging. Conventional routes rely on high-temperature melting or complex procedures, which are incompatible with delicate substrates and large-scale fabrication. Herein, we pioneer the fabrication of homogeneous, ultra-smooth glass-like MOF thin films, which can be readily scaled into large-area coatings via a facile room-temperature immersion strategy. By simply placing diverse substrates into the precursor solution for 0.5 to 3 hours, continuous amorphous MOF films with nanometer-scale flatness and centimeter-to-0.3-meter scale uniformity can be readily prepared, with exceptional mechanical properties including Young's modulus among the highest reported for typical ZIF glasses. Importantly, this unprecedented glass-like MOF film serves as a versatile guiding layer that enables the nucleation and growth of 15 different types of crystalline MOFs on various substrates, overcoming long-standing limitations of substrate dependence and lattice mismatch. This work not only establishes a facile and scalable synthetic platform for high-performance glass-like MOF thin films, but also extends its capability toward the universal growth of crystalline MOF films, unlocking promising new opportunities for device-oriented MOF thin-film materials for gas and isotope separation, electronic devices, sensing and electrocatalytic applications.

Introduction

Metal-organic frameworks (MOFs), a class of crystalline porous solids assembled from metal nodes and organic linkers, offer exceptional structural and chemical tunability.[1-3] With molecular-level control over topology, pore geometry, surface chemistry, and ultrahigh surface areas, MOFs are promising candidates for applications ranging from gas sorption[4,5] and molecular separation[6-8] to sensing,[9-11] catalysis,[12-14] and energy conversion.[15-17] To date, over 125,000 distinct MOF structures have been reported, with the vast majority existing as powdered polycrystals.[18] However, advancing MOFs toward practical applications necessitates their bulk processing or integration onto other material surfaces (e.g., films).[19-21] Given the inherent structural brittleness of MOFs and their prevalent polycrystalline form, the grain boundaries and intergranular cracks poses a major challenge to the fabrication of bulk MOFs or monolithic MOF films with high mechanic stability.[22]

The emergence of amorphous metal-organic frameworks,[23-25] particularly MOF glasses,[26-28] represents a critical advance in overcoming the processability limitations of conventional crystalline MOFs. These disordered yet structurally continuous materials intrinsically exhibit fracture resistance, high mechanical stability, and optical transparency.[29] In recent years, the synthesis of highly transparent, mechanically robust, and structurally continuous glassy MOFs has been achieved through post-synthetic amorphization of crystalline precursors via melt quenching or mechanochemical routes.[30,31] These structural characteristics endow MOF glasses with promising potential in applications such as gas separation,[32-34] catalysis[35-37] and energy storage system.[38-40] For instance, ZIF-62 glass membranes demonstrate CH_4 permeance values of 30,000-50,000 GPU (approximately two orders of magnitude higher than most existing materials), while maintaining excellent separation selectivity.[32] Nevertheless, research on MOF glasses remains in its early stages, with successful examples confined to a hand of zeolitic imidazolate frameworks (ZIFs).[26] The vast family of oxygen-containing MOFs has so far resisted glass formation via melt quenching approaches.[41-43] In addition, the demanding synthesis conditions, including inert-atmosphere processing, high-temperature melting, and rapid quenching hinder the integration of MOF glasses with fragile, thermally sensitive substrates and other substrates. Furthermore, the complicated top-down fabrication process poses significant challenges in achieving uniform, thickness-controlled glass-like MOF films, limiting their scalability and practical applications.

Herein, we report a straightforward one-step approach to deposit homogeneous, glass-like metal-organic framework films on various substrates with tunable thickness. Unlike conventional top-down processing routes, this diffusion-mediated strategy enables the uniform assembly of amorphous coordination networks across diverse surfaces, forming transparent and continuous coatings. In this work, using 1-vinylimidazole as a deprotonating agent and dissolved O_2 as an oxidant (**Figure 1a and S1**), the diffusion-mediated process provides continuous and controlled release of deprotonated 2,5-dihydroxyterephthalic acid (DOBDC) and iron (III) ions, thereby allowing precise regulation over the growth of the glass-like Fe-DOBDC ($_g$Fe-DOBDC) framework. The resulting films possess a smooth surface with a roughness of only

about 2 nm, along with a tunable thickness ranging from 50 to 200 nm. They also demonstrate remarkable mechanical properties, achieving a Young's modulus of up to 15 GPa, which surpasses all previously reported ZIF-based glasses. The method is also highly scalable and allows for film deposition over areas as large as 0.3 by 0.2 square meters. Notably, due to multiple interfacial interactions such as covalent bonding, hydrogen bonding, and van der Waals forces between deprotonated 2,5-dihydroxyterephthalic acid and iron (III) ions species and various substrates, the $_g$Fe-DOBDC films exhibit strong adhesion toward diverse surfaces. This enables their controlled growth on a wide range of substrates, including semiconductors (silicon wafers), inorganic substrates (glass, ITO, carbon cloth, AAO membrane, mica), metals (Cu foil, Ti mesh, stainless-steel sheets), and polymers (PET, polypropylene separators, polytetrafluoroethylene (PTFE)). The uniform $_g$Fe-DOBDC films not only show excellent compatibility with ion beam patterning but also serve as an adhesive interlayer to overcome the poor substrate affinity commonly encountered in crystalline MOF films. Using this approach, we have successfully grown more than ten types of crystalline MOFs, such as ZIF-L, ZIF-8, MIL-88, ZIF-67, HKUST-1, Cu-HHTP, $Ni_3[Fe(CN)_6]_2$, $Ni[Ni(CN)_4]$ and MOF-74 on various substrates. This work not only provides a robust route for synthesizing high quality glass-like MOF films, but also establishes a general and effective platform for the controlled growth of crystalline MOF films on arbitrary substrates, thereby accelerating the practical application of MOF-based materials.

Results and discussion

Controlled bottom-up assembly is essential for achieving uniform formation and growth of amorphous metal-organic frameworks. In this work, we target Fe-DOBDC as a model system to address the challenge of rapid, uncontrolled homogeneous nucleation that typically dominates the synthesis of amorphous coordination networks. To regulate the reaction kinetics, we developed a dual-diffusion mediated approach that independently modulates organic ligand and metal ion concentration. When Fe(II) ion and H_4DOBDC are mixed directly in methanol, the solution remains transparent even after 1h, with no detectable change in its UV-Vis absorption spectrum (**Figure S2**), indicating that the protonated ligand cannot effectively dissociate to form Fe-DOBDC metal-organic complexes. To modulate ligand deprotonation kinetics, we investigated a series of weak organic bases, including triethylamine (TEA), 2-methylimidazole (MIM), imidazole (IM), and 1-vinylimidazole (VIM) and evaluated their influence on the release of H_4DOBDC ligands. Theoretical simulations predict the proton-binding affinity of these bases to follow the order: triethylamine > 2-methylimidazole > imidazole > 1-vinylimidazole (**Figure 1b**). Deposition experiments on glass substrates align well with these predictions: stronger bases induce rapid deprotonation and dominant homogeneous nucleation, leading to poor film uniformity, whereas weaker bases favor heterogeneous nucleation and uniform deposition (**Figure S3**). Therefore, 1-vinylimidazole was selected as the optimal deprotonating agent. Upon addition of 1-vinylimidazole to the precursor solution, in situ UV-Vis absorption spectroscopy reveals the gradual formation of Fe-DOBDC metal-organic complexes, confirming that 1-vinylimidazole enables slow release of the organic linker and controlled growth of coordination networks (**Figure 1c and S4**). We further

optimized the deposition of Fe-DOBDC metal-organic complexes on glass substrates by adjusting the amount of 1-vinylimidazole, and achieved uniform deposition results (**Figure S5**). Simultaneously, dissolved oxygen acts as a mild oxidant to regulate the release of Fe(III) ions. Simulations show that the Fe(II)-O distance (~2.10 Å) is longer than that of Fe(III)-O (~2.02 Å), indicating weaker coordination of Fe(II) with DOBDC ligands.[44] Oxygen slowly oxidizes Fe(II) to Fe(III), promoting Fe-DOBDC complex formation. Such process is fully suppressed under argon (**Figure S6**), indicating the essential role of dissolved oxygen.

Molecular dynamics simulations further illustrate the process of Fe-DOBDC cluster formation and growth. In simulated methanolic box (**Figure 1d and 1e**), Fe(III) ion is firstly coordinated with Cl^- ions and methanol molecules. Then, the $DOBDC^{4-}$ anions gradually displace Cl^- ions and methanol molecules coordinated to Fe(III) ion, enabling gradual growth of Fe-DOBDC complexes. As shown in **Figure 1f and 1g**, the size of Fe-DOBDC clusters increases over time, evolving from freely dispersed ions into larger clusters containing 7 center metal ions. In contrast, protonated H_4DOBDC can only form monodentate structures incapable of extended network assembly (**Figure S7**). These results demonstrate that a dual-diffusion mediated strategy can regulate the kinetic of coordination bond formation and facilitate the uniform growth of Fe-DOBDC complexes.

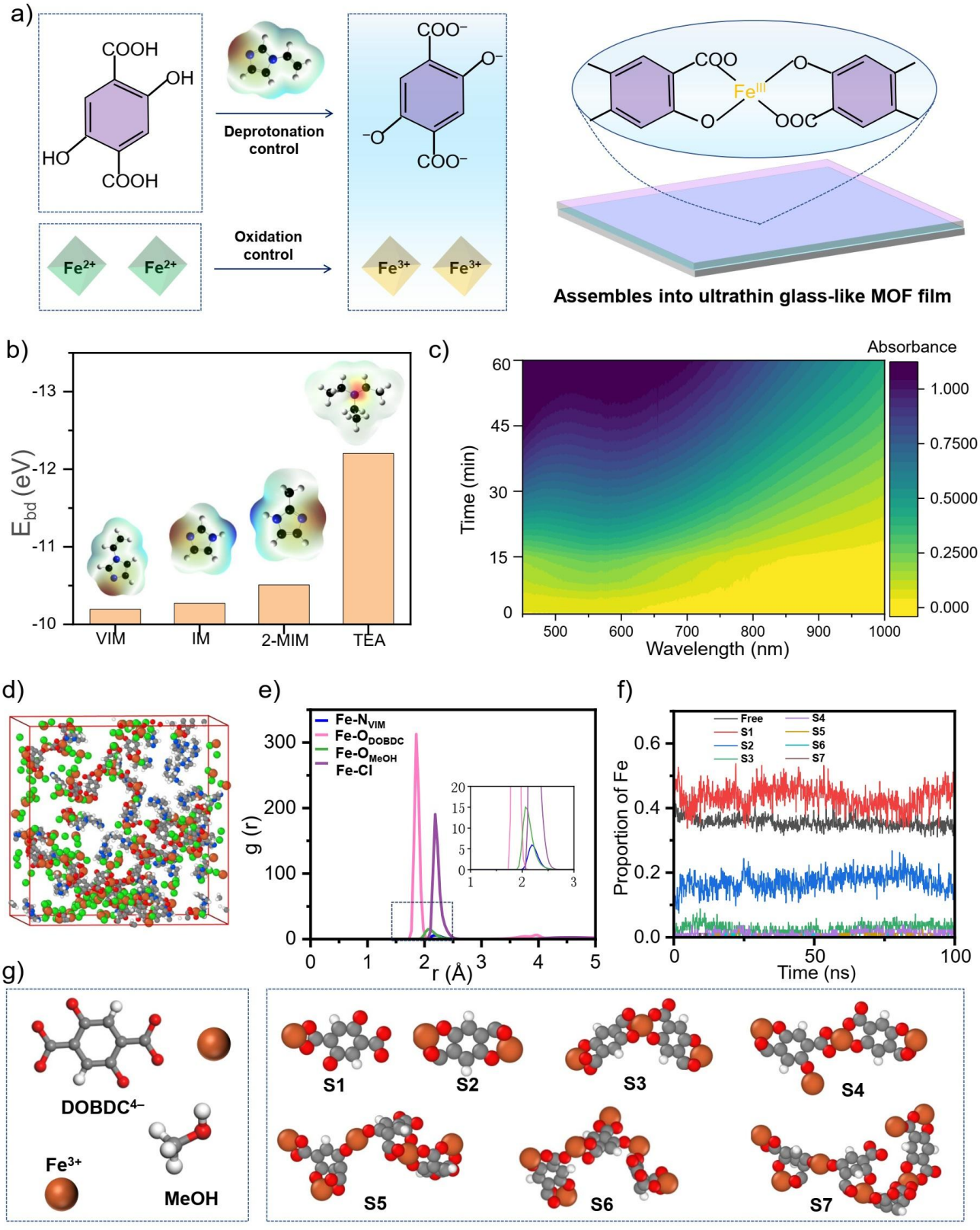


Figure 1. Kinetic control of Fe-DOBDC complexes assembly. (a) Schematic illustration of the dual-diffusion mediated strategy. (b) The proton binding energies of various weak organic bases. (c) Time-resolved in situ UV-vis absorption spectra of Fe-DOBDC complexes formation in the presence of 1-vinylimidazole. (d) Simulation box of the calculated system. The molar ratio of Fe^{3+}, Cl^{-}, 2,5-dihydroxyterephthalate (DOBDC), and 1-vinylimidazole was set to 48:96:12:26, with methanol employed as the solvent. Green spheres represent chlorine atoms, red spheres represent ferric ions, blue spheres represent nitrogen atoms, gray spheres represent carbon atoms, and white spheres represent hydrogen atoms. (e) Radial distribution functions of Fe(III) ions with respect to O atoms in DOBDC, O atoms in MeOH, N atoms in VIM, and Cl^{-} ions. (f) The distribution of Fe(III) ions in different cluster fractions over time. (g) Analysis and snapshots of Fe-DOBDC clusters of varying sizes.

The Powder X-ray diffraction (PXRD) pattern of Fe-DOBDC complexes shows a broad peak (**Figure 2a**), indicating its amorphous nature. After treating the amorphous Fe-DOBDC in N,N-Dimethylformamide at 180 °C for 20 h, it transforms into a crystalline state (**Figure 2a**), showing diffraction peaks consistent with crystalline MOF-74. Owing to the loss of long-range order in the structure, X-ray absorption spectroscopy (XAS) was used to clarify the local coordination environment of Fe in both amorphous and crystalline Fe-DOBDC. The X-ray absorption near-edge structure (XANES) spectra reveal nearly identical profiles for the two samples (amorphous and crystalline state), confirming their similar oxidation states. Fe predominantly exists as Fe(III), with α-Fe_2O_3 as the reference (**Figure 2b**). Fitting of the extended X-ray absorption fine structure (EXAFS) spectra provides average bond-length information of amorphous Fe-DOBDC complexes, which is consistent with those in the crystalline MOF-74 (**Figure 2c and Figure S8**). To further probe local atomic structures and short-range order, total X-ray scattering (TXS) combined with atomic pair distribution function (PDF) analysis were performed for both amorphous Fe-DOBDC and crystalline MOF-74. Comparing the PDFs below 8 Å (**Figure 2d**), the local structural motif of amorphous Fe-DOBDC resembles that of crystalline MOF-74, as the PDFs are highly similar. The observed atomic pair correlations of the PDFs are assigned to the interatomic distances present in a MOF-74 (**Figure 2e**). To probe the local chemical environment in both amorphous Fe-DOBDC and crystalline MOF-74, we performed Fourier-transform infrared (FTIR) and Raman spectroscopic analyses (**Figure S9**). The spectra demonstrate that amorphous Fe-DOBDC complexes exhibit spectral profiles nearly identical to its crystalline counterpart, implying highly similar coordination and bonding environments.

The thermal stability of amorphous Fe-DOBDC complexes was evaluated by thermogravimetric analysis (TGA) under an argon atmosphere. The TGA curve indicates that amorphous Fe-DOBDC retains good thermal stability, although it shows a slight decrease compared to its crystalline counterpart, attributable to the structural disorder (**Figure S10**). Pore characteristics and gas adsorption properties are key features of amorphous MOFs. N_2 and CO_2 adsorption measurements reveal that amorphous Fe-DOBDC exhibits weak N_2 uptake but pronounced CO_2 adsorption, reflecting a stronger chemical affinity between CO_2 and the coordination framework (**Figure 2f**). In contrast to the inert nature of N_2 molecules, the intrinsic polarity of CO_2 molecules enables chemical bonding interactions with the amorphous Fe-DOBDC framework. High-pressure CO_2 adsorption experiments demonstrate that the CO_2 uptake reaches 60 $cm^3\ g^{-1}$ at 30 bar (**Figure 2g**), indicating that gas molecules can efficiently access the internal voids of the disordered network under elevated pressure. Pore-size distribution derived from positron annihilation lifetime spectroscopy (PALS) (**Figure 2h**) shows that amorphous Fe-DOBDC maintains microporosity with a pore size of approximately 0.38 nm. These results suggest that, like most MOF glasses, amorphous Fe-DOBDC complexes lose long-range ordered porosity, yet the disordered network still contains accessible nanoscale voids.

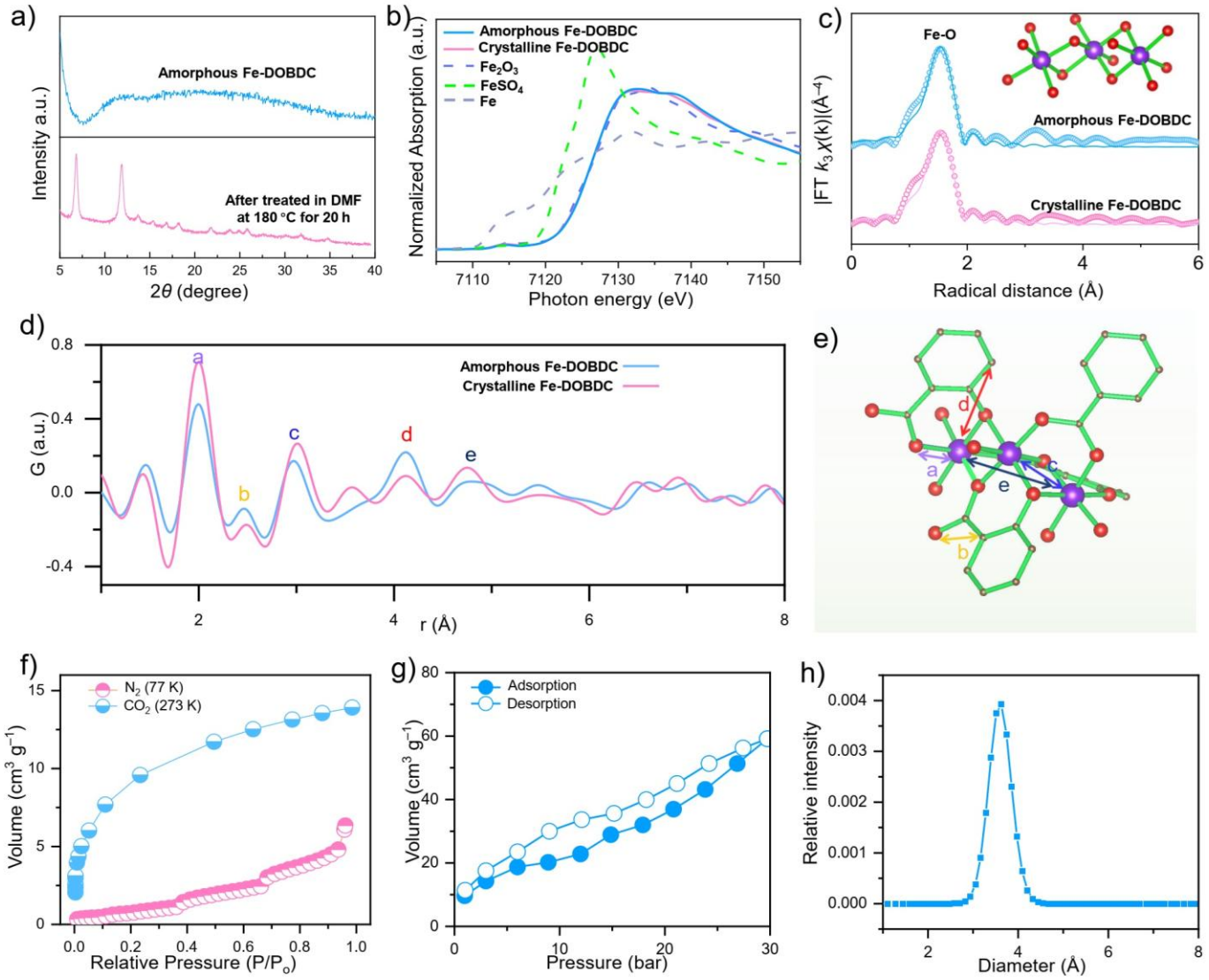


Figure 2. Structural characterization of amorphous Fe-DOBDC complexes. (a) PXRD patterns of amorphous Fe-DOBDC and the sample after DMF treatment at 180 °C for 20 h. The latter is consistent with crystalline MOF-74 (denoted as crystalline Fe-DOBDC). (b) Normalized XANES spectra of amorphous Fe-DOBDC and crystalline MOF-74. The curves of Fe foil, $FeSO_4$ and Fe_2O_3 are used as comparison, representing the valences of Fe^0, Fe^{2+} and Fe^{3+}, respectively. (c) The Fourier transform of Fe K-edge experimental EXAFS spectra of amorphous Fe-DOBDC and crystalline MOF-74. (d) Experimental pair distribution functions of amorphous Fe-DOBDC and crystalline MOF-74. (e) Atomic model of MOF-74 depicting interatomic distances that are highlighted in the PDF. The purple sphere represents Fe atom. The red sphere represents O atom. The dark-gray represents C atom. (f) N_2 sorption isotherm at 77 K and CO_2 sorption isotherm at 273 K of amorphous Fe-DOBDC. (g) CO_2 sorption isotherm at 273 K of amorphous Fe-DOBDC at high pressure. (h) Pore size distributions for amorphous Fe-DOBDC based on PALS analyses.

The uniform integration of MOF glasses into thin films or membranes with controlled thickness on various substrates remains a significant challenge. In this case, a mild dip-coating strategy was used to synthesize glass-like Fe-DOBDC (gFe-DOBDC) films through a controlled bottom-up assembly process. We first employed glass slide as a model substrate. The slide substrate was immersed in a methanolic solution containing Fe(II), H_4DOBDC, and 1-vinylimidazole, followed by static incubation at room temperature for 45 minutes. Subsequently, a uniform, dark transparent film formed on the surface (**Figure 3a**). This result indicates the successful growth of gFe-DOBDC layer. Scanning electron microscopy (SEM) images revealed that the film is continuous, flat, and uniform (**Figure 3a**). Atomic force microscopy (AFM) further demonstrated its nanoscale smoothness, with a roughness of only 2.6 nm and a thickness of approximately 65 nm (**Figure 3b**). X-ray reflectivity (XRR), a critical technique for characterizing film thickness and roughness, was employed to analyze the gFe-DOBDC film. The fitting results showed a thickness of 56 nm and a roughness of 0.8 nm, consistent with the AFM measurements (**Figure 3c**). Film thickness could be uniformly tuned from 30 to 200 nm by simply varying the incubation time. Systematic studies conducted at 30 min, 45 min, 1 h, 2 h, and 5 h showed that the gFe-DOBDC films maintained their glassy transparency (**Figure S11**). Differential scanning calorimetry analysis reveals that pristine Fe-DOBDC complexes exhibit no obvious glass transition temperature (**Figure S12**), and we therefore designate it as a glass-like thin film. Meanwhile, their optical transmittance gradually decreased with increasing thickness, which grew from 35 nm, to 65 nm, 125 nm, 155 nm, and finally 175 nm (**Figure 3d, 3f and S13-17**). Energy-dispersive X-ray spectroscopy (EDS) mapping revealed a homogeneous distribution of Fe, C and O across the coated region (**Figure 3e and S18**), and the cross-sectional SEM image also clearly depicted the continuous Fe-DOBDC layer (**Figure S19**), confirming the uniform deposition of gFe-DOBDC on the substrate.

The mechanical properties of MOF glasses, particularly Young's modulus and hardness, are critical for their practical application. Nanoindentation was employed to evaluate the mechanical performance of the film. The nearly overlapping load-displacement curves (**Figure 3g**) obtained from five randomly selected locations indicate excellent mechanical uniformity across the gFe-DOBDC film. The film exhibits a Young's modulus of 15 GPa (**Figure 3h**) and a hardness of 0.68 GPa (**Figure 3i**). [45,46] While the hardness is comparable to that of typical MOF glasses, the Young's modulus is significantly higher than most reported values for typical ZIF glasses (**Figure 3j**),[47-52] highlighting its superior mechanical properties. This enhancement is attributed to the diverse Fe-O coordination bonding environments in the Fe-DOBDC framework, which strengthens the material's resistance to deformation. Additionally, nanoscratch tests showed that noticeable film delamination began only after a scratch distance of 150 μm (**Figure S20**), demonstrating strong adhesion between the film and the substrate.

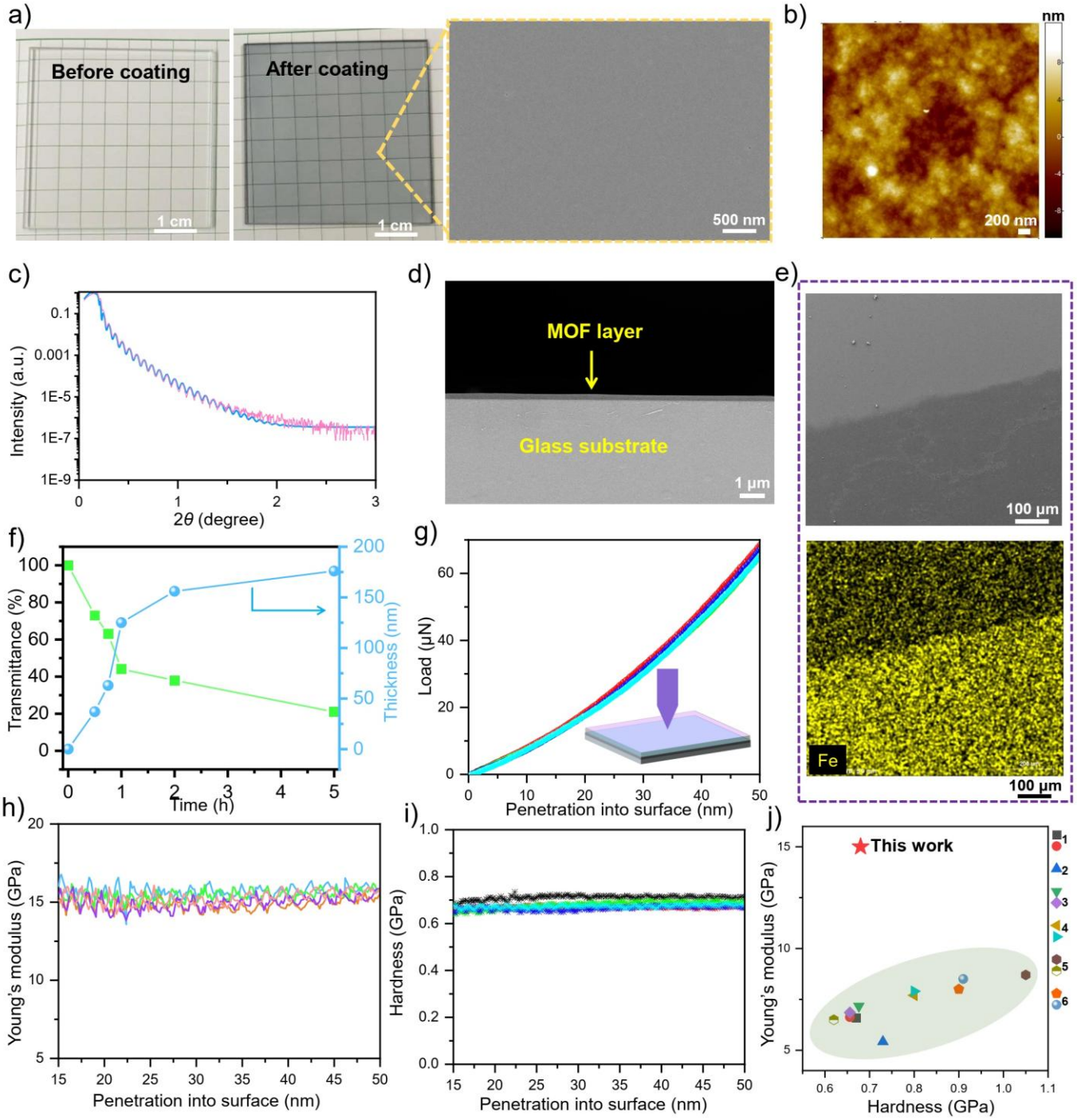


Figure 3. Preparation and characterization of gFe-DOBDC thin films. (a) Photograph of glass-like Fe-DOBDC film and corresponding SEM image. (b) AFM height image of the gFe-DOBDC film surface. (c) X-ray reflectivity analysis of the gFe-DOBDC film. The measured curve (blue line) and corresponding fitting (pink line). (d) Cross-sectional SEM image of the film. (e) EDS elemental mapping of the gFe-DOBDC film. Part of the area is masked in synthesis for comparison. (f) Evolution of film thickness and optical transmittance with reaction time. (g) Nanoindentation load-displacement curves of gFe-DOBDC film. Different colors represent randomly selected regions for testing. (h) Young's modulus as a function of indentation depth on gFe-DOBDC film. (i) The hardness as a function of indentation depth on gFe-DOBDC film. (j) Comparison of the E versus H of the gFe-DOBDC film with the typical MOF glasses. **1**: ref. 47; **2**: ref.48; **3**:ref 49; **4**:ref 50; **5**: ref.51; **6**: ref 52.

Developing glass-like MOF films on diverse substrates is of significant practical and technological relevance. To verify that our method is applicable irrespective of substrate surface chemistry or geometry (**Figure 4a-4b**), we tested a wide range of materials including stainless-steel battery cases, polytetrafluoroethylene (PTFE), a stone die, mica sheets, copper foil, ceramic crucibles, carbon cloth, polypropylene (PP) separators, single-crystal silicon wafers, porous anodic aluminum oxide (AAO) membranes, and flexible polyethylene terephthalate (PET). The selected substrates cover various geometries such as flat sheets, cylinders, cubes, and rectangles. After immersion in the reaction solution and static incubation at room temperature for 30 min to 2 h, the Fe-DOBDC films were successfully grown on all substrates, as clearly shown in the corresponding optical and SEM figures (**Figure 4b and S21-28**). These findings demonstrate that the deposition process is substrate-independent and possesses broad generality.

Additionally, a key advantage of MOF glasses over conventional glasses lies in their highly tunable molecular structures. To demonstrate the generality of our synthetic approach, we selected five different organic molecules as ligands while keeping the same synthesis strategy, simply replacing H_4DOBDC with structurally varied hydroxycarboxylic acids. As shown in **Figure 4c and S29**, thin films were successfully deposited on glass substrates in all cases, with each exhibiting good optical transparency. SEM images confirmed that all films display a smooth and uniform surface morphology and PXRD results demonstrate the amorphous nature of the as-prepared coordination polymers (**Figure S30, S32, S34, S36, and S37**). In contrast to the above gFe-DOBDC system, the different ligand molecules induce distinct intramolecular electron-transfer characteristics, resulting in different optical appearances, including purple, brown, and green as illustrated in **Figure 4c, S30, S32, S34, S36 and S37**. XANES spectra confirmed that iron remains predominantly in the +3 oxidation state in all coordination framework. Fitting of the extended EXAFS spectra clearly indicated the formation of Fe–O coordination bonds (**Figure S31, S33 and S35**). Furthermore, pair distribution function data revealed that the synthesized films exhibit short-range order similar to that of their crystalline counterparts. Notably, the intensity of the peak near 1.4 Å varies with the number of benzene rings in the ligand (increasing from one to three), corresponding to the nearest C–C distance within the molecule, which extends accordingly with the growing aromatic system (**Figure S31, S33 and S35**). These results confirm that the method can be extended to other Fe-hydroxycarboxylate systems for the preparation of high-quality glass-like MOF films.

Compared to other methods, this approach integrates multiple advantages that have not been simultaneously achieved in a single system (**Figure 4a**). First, it features mild synthesis conditions, relying solely on a simple room-temperature dip-coating process. Second, the precise control of reaction kinetics through a dual-diffusion mechanism enables the orderly and controllable assembly of Fe(III) ions and DOBDC linkers in solution, thereby ensuring the formation of uniform, high-quality films with tunable thickness. Furthermore, this method overcomes the limitation of conventional approaches in fabricating large-area films, as demonstrated by the successful preparation of a 0.2×0.3 m^2 film on flexible PET substrate. More importantly, the multiple interactions between hydroxycarboxylate and the substrates, including

covalent bonding, hydrogen bonding, and van der Waals forces, allowing stable film deposition on various substrates regardless of their surface properties and shape. The strategy is also readily extendable to other hydroxycarboxylate ligand systems. By combining operational simplicity, high product quality, scalability, substrate-independent deposition, and structural versatility, this method exhibits outstanding potential for practical applications.

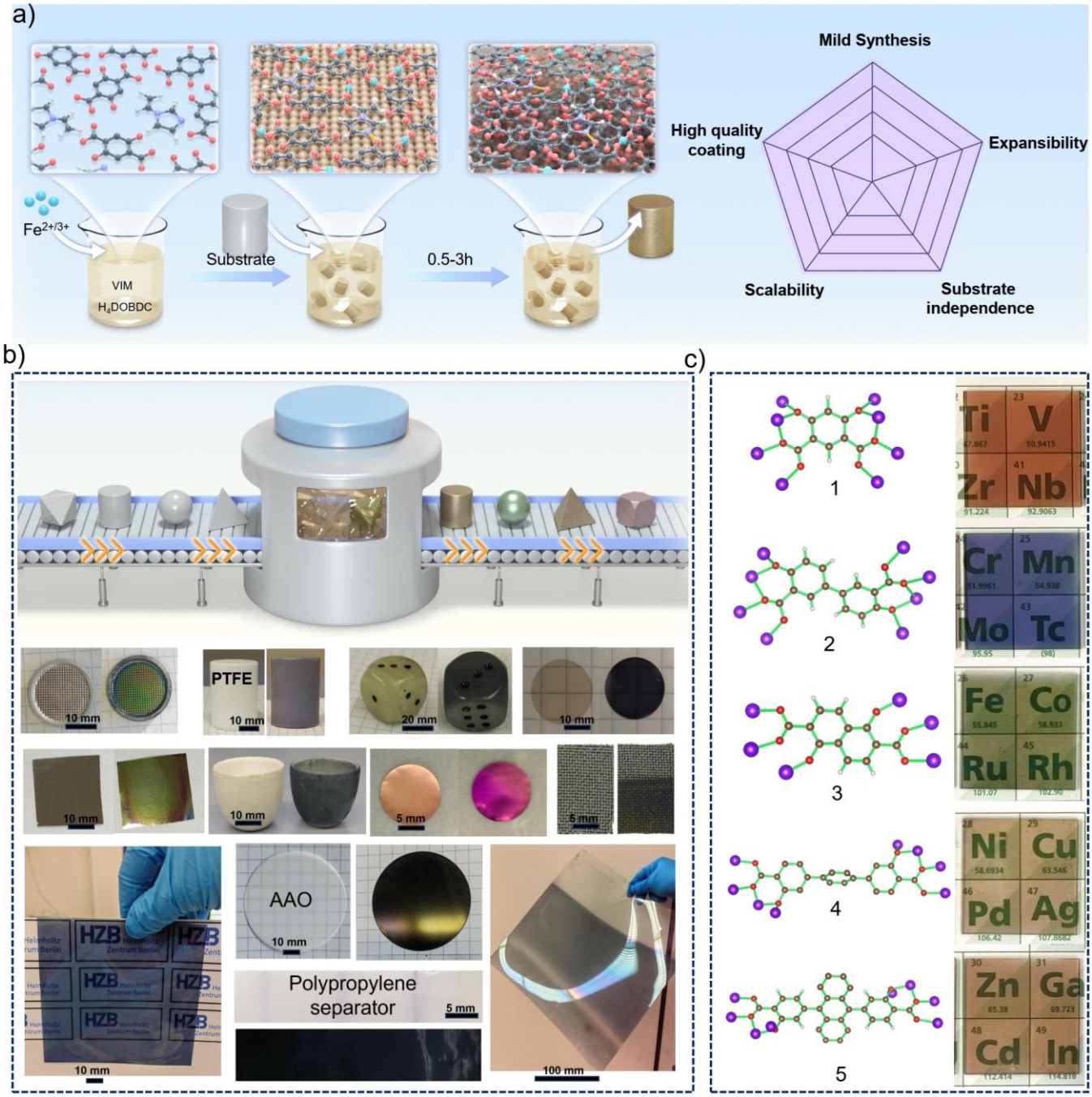


Figure 4. Demonstration of structural versatility and substrate-independent deposition. (a) Schematic illustration of gFe-DOBDC formation and deposition on diverse substrates and the radar chart summarizing the advantages of this diffusion-mediated synthesis strategy. The blue ball represents Fe atom. (b) Schematic illustration of thin films grown on various substrates. Photographs of glass-like Fe-DOBDC film on diverse substrates (coin cell case, PTFE rod, stone-carved dice, mica, stainless-steel sheet, crucible, Cu foil, carbon cloth, PET, silicon wafers, AAO membrane, polypropylene separator, large-area PET substrate). The film layer is black in color and a few samples exhibit other colors due to structural coloration caused by thin-film interference. (c) Extension to other hydroxycarboxylate ligand system. The elements under the transparent film are purely illustrative to visualize its high transparency and have no scientific implication. The side length of the square ITO substrate is 20 mm.

The potential applications of glass-like gFe-DOBDC thin films will be introduced. Firstly, their amorphous structural nature endows the films with a high concentration of defect sites that exhibit strong affinity toward metal ions. In lithium metal batteries, the weak affinity between lithium ions and copper current collectors affects the kinetics of lithium deposition, often leading to lithium dendrite growth. To address this, a layer of gFe-DOBDC film was fabricated on the surface of copper foil. Experimental results show that the gFe-DOBDC-coated copper exhibits a distinct color change and pronounced structural coloration (**Figure S38**). As the coating time increases, the roughness of the original copper surface decreases significantly, confirming the high-quality growth of the gFe-DOBDC film on the copper substrate. Compared with pure copper, the oxygen-containing functional groups in gFe-DOBDC possess higher lithium adsorption energy (**Figure 5a**). In Li-Cu asymmetric cell tests, the gFe-DOBDC-coated copper electrode demonstrates superior coulombic efficiency. The gFe-DOBDC-modified electrode maintains stable performance even after 150 cycles, while the coulombic efficiency of bare copper declines sharply after 50 cycles (**Figure S4b**). This is primarily ascribed to the enhanced lithiophilicity of the gFe-DOBDC modified Cu foil, which favors lithium deposition (**Figure S39**). In full-cell tests with $LiFePO_4$ cathodes, the gFe-DOBDC film also exhibits excellent electrochemical stability (**Figure S40**). Furthermore, the patterning of MOF films is crucial for applications in electronics, optics, and related fields, which typically require high film quality.[47-48] This work demonstrates the successful patterning of gFe-DOBDC films. Using ion beam lithography, various patterns such as stripes, square arrays, and even custom shapes or characters can be precisely created **(Figure 5c**). Looking forward, gFe-DOBDC films hold promise for further processing with lasers or electron beams, extending their potential applications in the semiconductor industry.

The growth of crystalline MOF thin films represents a vital challenge in realizing their practical applications. However, the diverse surface properties of substrates have hindered the development of a generalizable synthesis strategy. Here, we employ a gFe-DOBDC layer as a functional interfacial modifier to promote the adsorption, nucleation, and growth of various crystalline MOFs. The metal nodes and organic ligands within gFe-DOBDC provide multiple adsorption sites for MOF precursors. Taking the $Co_3[Fe(CN)_6]_2$ (Prussian blue analogue) as an example (**Figure 6a and S41**), we placed pristine glass and gFe-DOBDC-modified glass substrates into the same reaction solution. After five minutes, the unmodified substrate remained unchanged, whereas the gFe-DOBDC-modified glass exhibited vivid structural coloration (**Figure S42**). SEM images revealed a dense layer of cubic crystals on the surface, and powder X-ray diffraction patterns confirmed a perfect match with crystalline $Co_3[Fe(CN)_6]_2$ (**Figure 6b and S41**). These results demonstrate the successful deposition of a highly crystalline $Co_3[Fe(CN)_6]_2$ thin film induced by the gFe-DOBDC interlayer. Subsequently, gFe-DOBDC modification layers were fabricated on a variety of substrates, including AAO, carbon cloth, Cu foil, PET, Ti, stainless steel, Si wafer, and PP separator (**Figure 5c and 5d**). Upon immersion in the reaction solution for merely 5 min, highly crystalline $Co_3[Fe(CN)_6]_2$ thin films were grown on all substrates (**Figure S43-S50**), validating the versatility of this approach for depositing crystalline thin films on diverse surfaces.

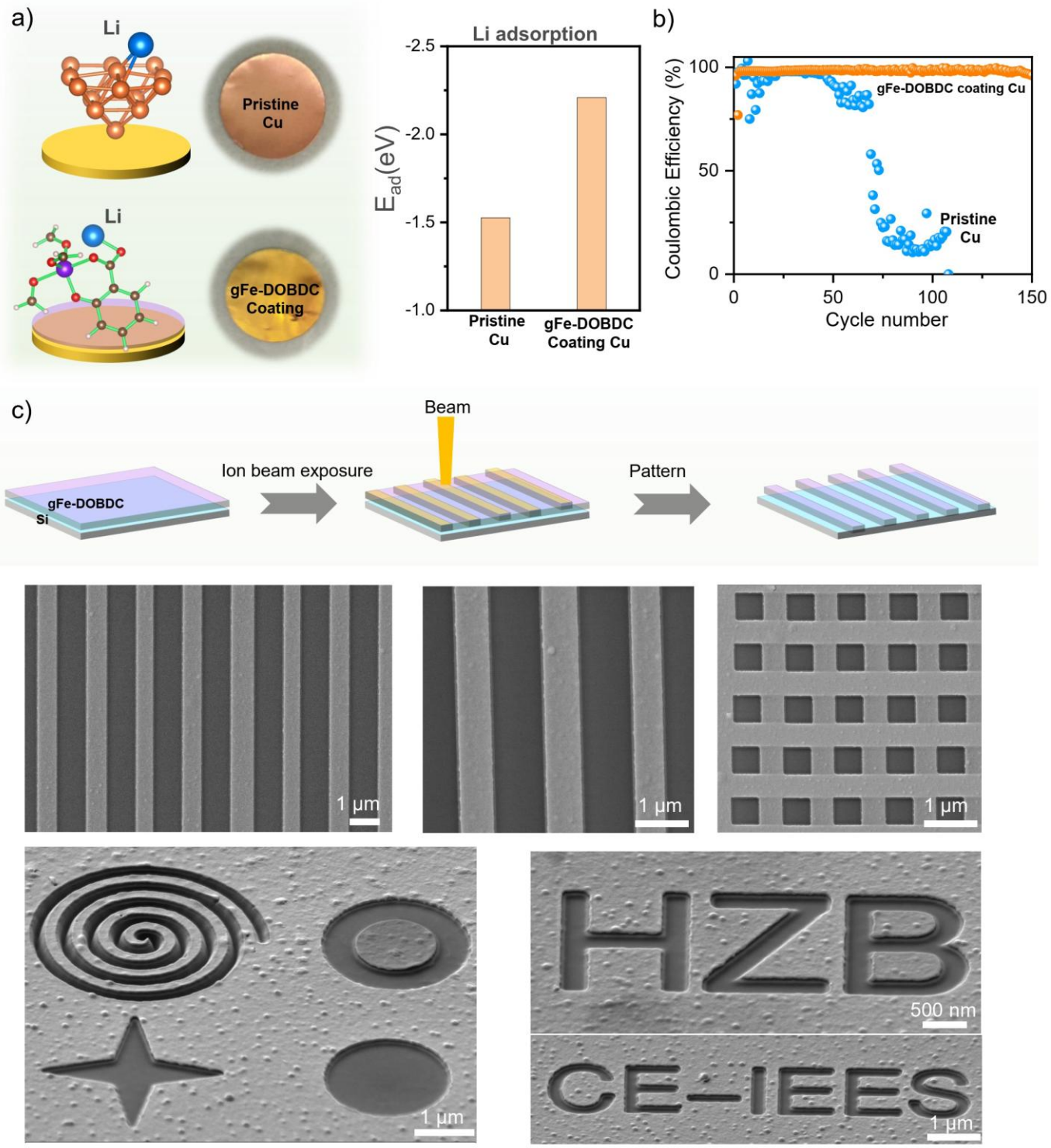


Figure 5. Application of gFe-DOBDC thin films. (a) Photograph of pristine Cu plate and gFe-DOBDC thin film coated on Cu and the calculated adsorption energies of Li with gFe-DOBDC and Cu. (b) Comparison of coulombic efficiency for pristine Cu plate and gFe-DOBDC thin film on Cu. (c) A schematic illustration of ion beam lithography patterning of gFe-DOBDC thin film and corresponding SEM images.

To validate the generality of this approach across diverse crystalline MOFs, we also extended the method to MOFs and coordination polymers with diverse topologies, including ZIF-L-Co, ZIF-L-Zn, ZIF-8, ZIF-67, HKUST-1, MIL-88, Cu-HHTP, MOF-74, Cu-NH_2-BDC, $Mn_3[Co(CN)_6]_2$, $Ni_3[Fe(CN)_6]_2$, $Ni[Ni(CN)_4]$, and $Ag[Ag(CN)_2]$. Using gFe-DOBDC as a universal functional layer, we successfully obtained thin films of all 14 distinct materials (**Figure S51-S64**). SEM and optical images clearly reveal the formation of various MOF thin films. Moreover, given that gFe-DOBDC can be deposited on various substrates, this methodology theoretically enables the growth of diverse crystalline MOFs on virtually any surface. This work thus provides a versatile and generalizable platform for the controllable fabrication of MOF thin films, paving the way for their integration into advanced electronic, optical, and semiconductor devices.

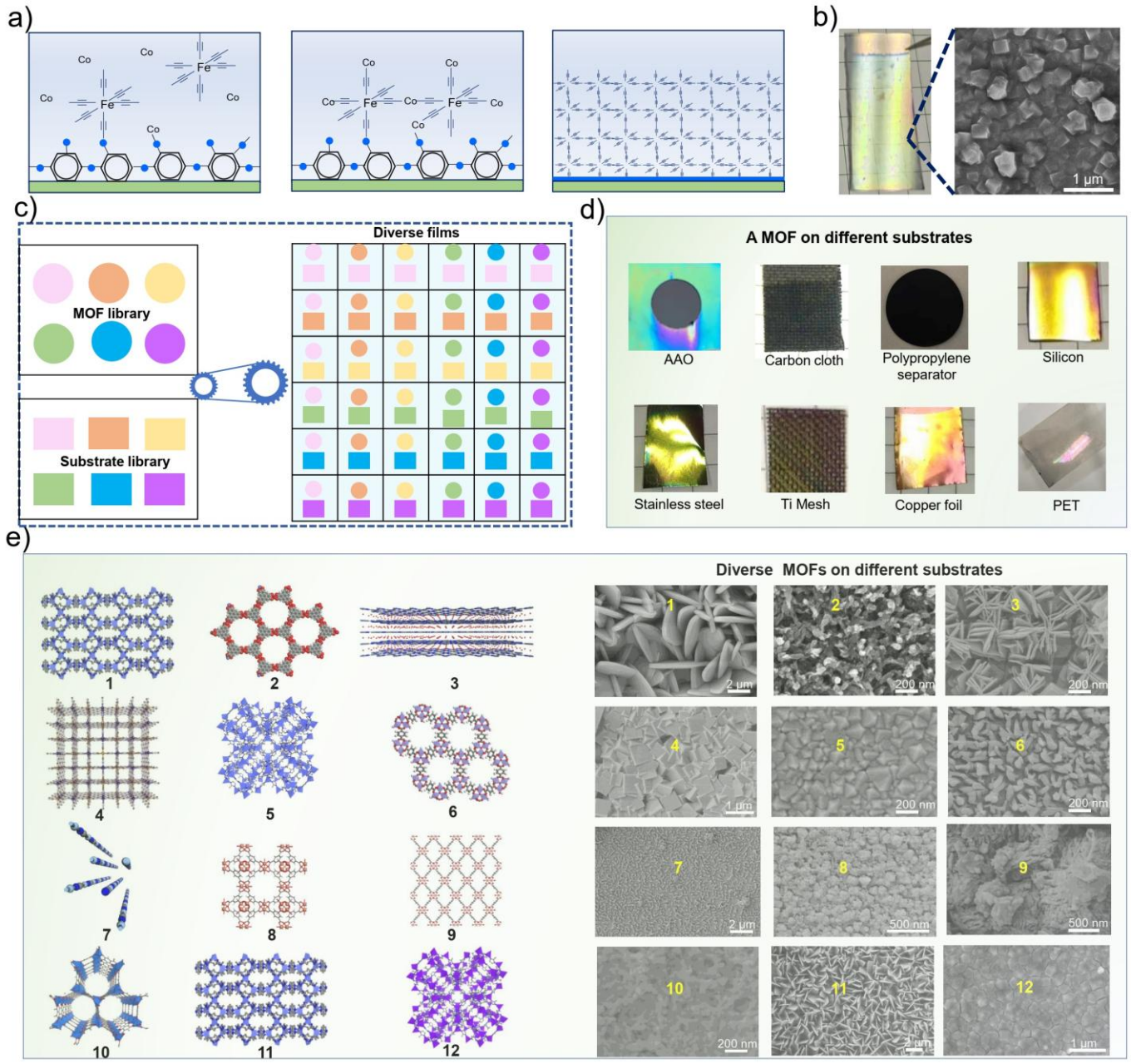


Figure 6. Synthesis of Diverse Crystalline MOF films. (a) Schematic illustration of the growth of $Co_3[Fe(CN)_6]_2$ thin film on gFe-DOBDC modified substrate. (b) Photograph and SEM image of $Co_3[Fe(CN)_6]_2$ thin film on glass. (c) Schematic illustration of diverse MOFs deposited on different substrates. (d) $Co_3[Fe(CN)_6]_2$ thin film on various substrates. (e) Diverse crystalline MOF films. ZIF-L-Co (**1**), Cu-HHTP (**2**), $Ni[Ni(CN)_4]$ (**3**), $Mn_3[Co(CN)_6]_2$ (**4**), ZIF-8 (**5**), MIL-88 (**6**), $Ag[Ag(CN)_2]$ (**7**), HKUST-1 (**8**), Cu-NH_2-BDC (**9**), MOF-74 (**10**), ZIF-L-Zn (**11**), and ZIF-67(**12**).

Conclusion

In this work, we have established a comprehensive and versatile platform for the design, synthesis, functionalization, and integration of glass-like Fe-DOBDC thin films. 1-vinylimidazole as a deprotonating agent and dissolved O_2 as an oxidant are used to provide continuous and controlled release of deprotonated 2,5-dihydroxyterephthalic acid (DOBDC) and iron (III) ions, thereby regulating the bottom-up assembly kinetics. The dual-diffusion synthetic method enables precise control over film thickness, uniformity, and microstructure, providing a robust foundation for large-scale fabrication. Through advanced local structural characterization, including X-ray absorption spectroscopy and pair distribution function analysis, we confirm that the local structure of gFe-DOBDC is characterized by a preserved short-range coordination environment alongside long-range disorder. The method enables controlled film growth on diverse substrates, including silicon, glass, metals, carbon cloth and flexible polymers through multiple interfacial interactions between hydroxycarboxylate molecules and the substrate surface. The obtained glass-like films are highly transparent and structurally continuous, with a Young's modulus reaching 15 GPa. This represents one of the highest Young's modulus values reported for MOF-based glasses. Furthermore, the gFe-DOBDC films can serve as a universal adhesion promoting interlayer, overcoming the substrate compatibility limitations of crystalline MOFs. Using this platform, we have successfully grown 14 types of crystalline MOFs and coordination polymers, such as ZIF-L-Co, ZIF-L-Zn, ZIF-8, ZIF-67, HKUST-1, MIL-88, Cu-HHTP, MOF-74, Cu-NH_2-BDC, $Ni_3[Fe(CN)_6]_2$, $Ni[Ni(CN)_4]$, and $Ag[Ag(CN)_2]$ on various surfaces. In addition, the films are compatible with high-resolution patterning techniques, supporting their integration into functional devices. This work not only provides a robust synthesis route for high-quality glass-like MOF films but also establishes a versatile platform for the controlled growth of crystalline MOF films on arbitrary substrates, accelerating the practical application of MOF-based materials in electronics, energy storage, and beyond.

Data availability

The work's findings are backed by data presented in the article and its Supplementary Information files. Datasets can be obtained from the corresponding authors upon request.

Acknowledgements

This work was supported by the Startup Research Fund of Shanghai University. Q.W. acknowledges Alexander von Humboldt's research fellowship. We thank Dr. Nikolai Severin from Humboldt Universität Berlin for AFM measurements and Rene Schwiddessen from Helmholtz Zentrum Berlin für Materialien und Energie for XRR. We acknowledge DESY (Hamburg, Germany), a member of the Helmholtz Association HGF, for the provision of experimental facilities. Parts of this research were carried out at PETRA III. Data were collected using the Powder Diffraction and Total Scattering

Beamline P02.1 operated by DESY Photon Science. Beamtime was allocated for the proposal (Proposal No. I-20230735) and for in-house research.

Author contributions

All authors contributed to the preparation of this manuscript and approved the final version for publication. W.Z. and Y.L. conceived the project; Material synthesis, material characterization and data analysis was performed by W.Z.; J.S. and YC.L. assisted in the acquisition and analysis of XAS data. Battery test was performed by W.Z. and P.Q.; L.L. carried out the FIB experiments. The theoretical simulations and calculations were performed by Z.Z. M.A.K. performed TXS measurement and processed the data to generate PDFs. W.Z., N.P. and Y.L. wrote the manuscript. All authors have approved the manuscript.

Competing interests

The authors declare no competing interests.

References

1. Furukawa, H., Cordova, K. E., O'Keeffe, M. & Yaghi, O. M. The Chemistry and Applications of Metal-Organic Frameworks. *Science* **341**, 1230444 (2013).
2. Horike, S., Shimomura, S. & Kitagawa, S. Soft porous crystals. *Nat. Chem.* **1**, 695-704 (2009).
3. Farha, O. K. et al. Metal-Organic Framework Materials with Ultrahigh Surface Areas: Is the Sky the Limit? *J. Am. Chem. Soc.* **134**, 15016-15021 (2012).
4. Ye, Z. M. et al. Architecting Metal-Organic Frameworks at Molecular Level toward Direct Air Capture. *J. Am. Chem. Soc.* **147**, 5495-5514 (2025).
5. Carsch, K. M. et al. Multigas adsorption with single-site cooperativity in a metal–organic framework. *Science* **390**, 808-812 (2025).
6. Knebel, A. & Caro, J. Metal–organic frameworks and covalent organic frameworks as disruptive membrane materials for energy-efficient gas separation. *Nat. Nanotechnol.* **17**, 911-923 (2022).
7. Zhou, S. et al. Asymmetric pore windows in MOF membranes for natural gas valorization. *Nature* **606**, 706-712 (2022).
8. Liu, G. et al. Eliminating lattice defects in metal–organic framework molecular-sieving membranes. *Nat. Mater.* **22**, 769-776 (2023).
9. Kreno, L. E. et al. Metal–organic framework materials as chemical sensors. *Chem. Rev.* **112**, 1105-1125 (2012).
10. del Castillo-Velilla, I. et al. Synergistic binding sites in a metal-organic framework for the optical sensing of nitrogen dioxide. *Nat. Commun.* **14**, 2506 (2023).
11. Zhou, Z. et al. Porphyrinic MOF film for multifaceted electrochemical sensing. *Angew. Chem. Int. Ed.* **60**, 20551-

20557 (2021).

12. Zhong, H. et al. Synergistic electroreduction of carbon dioxide to carbon monoxide on bimetallic layered conjugated metal-organic frameworks. *Nat. Commun.* **11**, 1409 (2020).
13. Sun, K. et al. Dynamic structural twist in metal–organic frameworks enhances solar overall water splitting. *Nat. Chem.***16**, 1638-1646 (2024).
14. Zhao, X. *et al.* Bifunctional electrocatalysts for overall water splitting from an iron/nickel-based bimetallic metal–organic framework/dicyandiamide composite. *Angew. Chem. Int. Ed.* **130**, 9059-9064 (2018).
15. Salunkhe, R. R., Kaneti, Y. V. & Yamauchi, Y. Metal-Organic Framework-Derived Nanoporous Metal Oxides toward Supercapacitor Applications: Progress and Prospects. *ACS Nano* **11**, 5293-5308 (2017).
16. Sheberla, D. et al. Conductive MOF electrodes for stable supercapacitors with high areal capacitance. *Nat. Mater.* **16**, 220-224 (2017).
17. Wang, H. F., Chen, L. Y., Pang, H., Kaskel, S. & Xu, Q. MOF-derived electrocatalysts for oxygen reduction, oxygen evolution and hydrogen evolution reactions. *Chem. Soc. Rev.* **49**, 1414-1448 (2020).
18. Pruyn, T. M. *et al.* MOF-ChemUnity: Literature-Informed Large Language Models for Metal–Organic Framework Research. *J. Am. Chem. Soc.* **147**, 43474-43486 (2025).
19. Ji, Y.-L. et al. Roll-to-roll fabrication of large-area metal–organic framework-based membranes for high-performance aqueous separations. *Nat. Water* **2**, 183-192 (2024).
20. Shekhah, O., Liu, J., Fischer, R. & Wöll, C. MOF thin films: existing and future applications. *Chem. Soc. Rev.* **40**, 1081-1106 (2011).
21. Wright, A. M., Kapelewski, M. T., Marx, S., Farha, O. K. & Morris, W. Transitioning metal-organic frameworks from the laboratory to market through applied research. *Nat. Mater.* **24**, 178-187 (2025).
22. Lin, Z., Richardson, J. J., Zhou, J. & Caruso, F. Direct synthesis of amorphous coordination polymers and metal–organic frameworks. *Nat. Rev. Chem.* **7**, 273-286 (2023).
23. Zhang, W., Liu, Y., Jeppesen, H. S. & Pinna, N. Stöber method to amorphous metal-organic frameworks and coordination polymers. *Nat. Commun.* **15**, 5463 (2024).
24. Mahdavi, H. et al. Practical Considerations in the Design and Use of Non-Crystalline Metal-Organic Frameworks. *Adv. Mater.* **37**, e05579 (2025).
25. Bennett, T. D. & Horike, S. Liquid, glass and amorphous solid states of coordination polymers and metal-organic frameworks. *Nat. Rev. Mater.* **3**, 431-440 (2018).
26. Wei, Y. S., Ashling, C. W., Watcharatpong, T., Fan, Z. & Horike, S. Hierarchical metal-organic network-forming glasses toward applications. *Adv. Funct. Mater.* **34**, 2307226 (2024).
27. Bennett, T. D., Horike, S., Mauro, J. C., Smedskjaer, M. M. & Wondraczek, L. Looking into the future of hybrid

glasses. *Nat. Chem.* **16**, 1755-1766 (2024).

28. Qiao, A. *et al.* A metal-organic framework with ultrahigh glass-forming ability. *Science advances* **4**, eaao6827 (2018).
29. Ma, N. & Horike, S. Metal–organic network-forming glasses. *Chem. Rev.* **122**, 4163-4203 (2022).
30. Tao, H., Bennett, T. D. & Yue, Y. Melt-quenched hybrid glasses from metal–organic frameworks. *Adv. Mater.* **29**, 1601705 (2017).
31. Xue, W.-L. et al. Melt-quenched glass formation of a family of metal-carboxylate frameworks. *Nat. Commun.* **15**, 2040 (2024).
32. Yang, Z. et al. ZIF-62 glass foam self-supported membranes to address CH4/N2 separations. *Nat. Mater.* **22**, 888-894 (2023).
33. Smirnova, O. et al. Precise control over gas-transporting channels in zeolitic imidazolate framework glasses. *Nat. Mater.* 23, 262-270 (2024).
34. Xie, S. et al. Cathodic Deposition-Assisted Synthesis of Thin Glass MOF Films for High-Performance Gas Separations. *Angew. Chem. Int. Ed.* **136**, e202401817 (2024).
35. Huang, W. *et al.* Intermarrying MOF glass and lead halide perovskites for artificial photosynthesis. *J. Am. Chem. Soc.* **147**, 3195-3205 (2024).
36. Kosasang, S. et al. Prussian blue analogue glasses for photoinduced CO2 conversion. *J. Am. Chem. Soc.* **146**, 17793-17800 (2024).
37. Song, Y. et al. Metal-organic framework glass catalysts from melting glass-forming cobalt-based zeolitic imidazolate framework for boosting photoelectrochemical water oxidation. *Angew. Chem. Int. Ed.* **62**, e202306420 (2023).
38. Gao, C. et al. Metal-organic framework glass anode with an exceptional cycling-induced capacity enhancement for lithium-ion batteries. *Adv. Mater.* **34**, 2110048 (2022).
39. Chen, W. et al. Glass formation of a coordination polymer crystal for enhanced proton conductivity and material flexibility. *Angew. Chem. Int. Ed.* **128**, 5281-5286 (2016).
40. Bai, L. *et al.* Metal-organic framework glass stabilizes high-voltage cathodes for efficient lithium-metal batteries. *Nat. Commun.* **16**, 3484 (2025).
41. Albolkany, M. K., Cui, S., Zhao, Y. & Liu, B. A Capping-assisted Strategy for Synthesis of Glass-like Carboxylate-based Coordination Polymers. *Angew. Chem. Int. Ed.* **64**, e202500266 (2025).
42. Wei, Y.-S., Fan, Z., Luo, C. & Horike, S. Desolvation of metal complexes to construct metal–organic framework glasses. *Nat. Syn.* **3**, 214-223 (2024).
43. Zhang, Z. & Zhao, Y. Transparent and high-porosity aluminum alkoxide network-forming glasses. *Nat. Commun.*15, 7339 (2024).
44. Remsungnen, T. & Rode, B. M. QM/MM molecular dynamics simulation of the structure of hydrated Fe(II) and Fe(III)

ions. *J. Phys. Chem. A* **107**, 2324–2328 (2003).

45. Widmer, R. N., Bumstead, A. M., Jain, M., Bennett, T. D. & Michler, J. Plasticity of Metal-Organic Framework Glasses. *J. Am. Chem. Soc.* **143**, 20717-20724 (2021).
46. Tian, T. et al. A sol-gel monolithic metal-organic framework with enhanced methane uptake. *Nat. Mater.* **17**, 174-179 (2018).
47. Li, S. et al. Highly porous metal-organic framework glass design and application for gas separation membranes. *Nat. Commun.* **16**, 1622 (2025).
48. Li, S. et al. Ionic liquid facilitated melting of the metal-organic framework ZIF-8. *Nat. Commun.* **12**, 5703 (2021).
49. Li, S. et al. Mechanical properties and processing techniques of bulk metal–organic framework glasses. *J. Am. Chem. Soc.* **141**, 1027–1034 (2019).
50. Hou, J. et al. Metal-organic framework crystal-glass composites. *Nat. Commun.* **10**, 2580 (2019).
51. Bennett, T. D. et al. Structure and properties of an amorphous metal–organic framework. *Phys. Rev. Lett.* **104**, 125505 (2010).
52. Bennett, T. D. et al. Melt-quenched glasses of metalorganic frameworks. *J. Am. Chem. Soc.* **138**, 3494–3501 (2016)
53. Miao, Y. R. et al. Spin-on deposition of amorphous zeolitic imidazolate framework films for lithography applications. *Nature Chemical Engineering* **2**, 594-607 (2025).
54. Tian, X. L. et al. Crosslinking-induced patterning of MOFs by direct photo- and electron-beam lithography. *Nat. Commun.* **15**, 2920 (2024).

Supplementary Files

This is a list of supplementary files associated with this preprint. Click to download.

- SupplementaryS.pdf